Computational Mechanics (2019) 63:471–489
https://doi.org/10.1007/s00466-018-1604-7

ORIGINAL PAPER

Encapsulated piezoelectric nanoparticle–hydrogel smart material to remotely regulate cell differentiation and proliferation: a finite element model

S. Jamaleddin Mousavi[1,2,3] · Mohamed Hamdy Doweidar[1,2,3]

Received: 31 October 2017 / Accepted: 7 July 2018 / Published online: 17 July 2018

Abstract
Regenerative medicine is one of the most promising future approaches for the treatment of damaged tissues and organs. Its methodologies are based on a good understanding and control of cellular behavior within in-vivo tissues, and this represents an important challenge. Cell behavior can be controlled, among other stimuli, by changing the mechanical properties of the extracellular matrix, applying external/internal forces, and/or reproducing an electric stimulus. To remotely control the local cell micro-environment, we consider in this work a microsphere of cell size made of a piezoelectric material and charged with nanomagnetic particles. This microsphere is integrated within an extracellular matrix, in such a way that internal forces can be generated within the microsphere by means of an external magnetic field. As a result, a stiffness gradient and an electric field are generated around the microsphere. These stimuli can be controlled externally by changing the magnetic field intensity and direction. To fine-tune this process and achieve the desired cell numbers, a computational numerical simulation has been developed and employed for several cell phenotypes using the ABAQUS software with the user-define subroutine UEL. The 3D numerical model presented can successfully predict the fundamental aspects of cell maturation, differentiation, proliferation, and apoptosis within a nonlinear substrate. The results obtained, which are in agreement with previous experimental and computational works, show that the generated stiffness gradient as well as the electric field within the cell micro-environment can play a highly significant role in remotely controlling the lineage specification of the Mesenchymal Stem Cells and accelerating cell migration and proliferation, which opens the door to new methodologies of tissue regeneration.

Keywords Regenerative medicine · Differentiation and proliferation · Signals-induced matrices · Piezoelectric material · Mechanotaxis · Electrotaxis · Finite element method

1 Introduction

Due to the potential capability of Stem Cells (SCs) to differentiate and proliferate, multiple tissues can be generated from a single cell source. However, any misprogrammed differentiation of SCs can sometimes lead to disaster if they differentiate into undesired phenotypes in an inappropriate place and/or time, causing a pathological state or non-functional tissue construction. To prevent such abnormalities, cells have to be particularized in such a way that they differentiate or proliferate in response to appropriate biological stimuli. Innovative methods to trigger SC differentiation are highly promising for tissue engineering applications. Many factors may contribute to controlling the fate of SCs. For example, the employment of external cues is a potentially viable approach to induce differentiation of SCs in tissue engineering [1]. In particular, there is strong evidence sup-

Electronic supplementary material The online version of this article (https://doi.org/10.1007/s00466-018-1604-7) contains supplementary material, which is available to authorized users.

✉ Mohamed Hamdy Doweidar
mohamed@unizar.es

[1] Mechanical Engineering Department, School of Engineering and Architecture (EINA), University of Zaragoza, Zaragoza, Spain

[2] Aragón Institute of Engineering Research (I3A), University of Zaragoza, Zaragoza, Spain

[3] Biomedical Research Networking Center in Bioengineering, Biomaterials and Nanomedicine (CIBER-BBN), Zaragoza, Spain

porting the key role of physical cues, such as mechanical forces and electrical signals, in the determination of the fate of SCs [2]. Mechanical forces may include residual stresses, deformational loading and/or fluidic forces. The effect of electrical signals which generate electromotive forces are observed in many functions of living cells such as migration [3–5], differentiation and proliferation [6,7]. Control of SC migration and differentiation is considered vital during efficient SC therapy in which an electric field is an appropriate possibility for controlling its fate [6].

Experimentally, it has been proven that the mechanical structure of the cell micro-environment plays a significant role in cell differentiation and proliferation [8–11]. For instance, tissue rigidity induces Mesenchymal Stem Cells (MSCs) to differentiate into specific phenotypes. The mechanical interaction between a cell and its Extracellular Matrix (ECM) can be considered as an asymbiotic process which means a dynamic reciprocity relationship [12]. Consequently, in addition to other cell reactions [13–16], cells are programmed to react to any alteration of their matrix by undergoing differentiation and/or proliferation [12,17]. Many studies [12,18–20] have demonstrated that hard matrices mimicking a tissue of collagenous bone of collagenous bone (with ECM stiffness of 30–45 kPa) induce SCs to differentiate into osteogenic cells, intermediate matrices resembling cartilage tissue of collagenous bone (with ECM stiffness of 20–25 kPa) induce them to differentiate into chondrogenic cells while relatively soft matrices mimicking brain tissue (with ECM stiffness of 0.1–1 kPa) induce them to differentiate into neurogenic cells. It is worth noting that quicker differentiation and higher proliferation rates of MSCs are observed when they are cultured on osteogenic ECM with the upper value of the corresponding stiffness bound [19,21,22]. Kurpinsk et al. [23,24] have observed that mechanical forces induced into the cell micro-environment can essentially be responsible for these processes. They indicate that mechanical strains, induced by external forces, increase MSC proliferation and have important implications for MSC differentiation. Besides, they indicate that the differential cellular responses to an anisotropic mechanical environment in a force-induced micro-environment play an important role in tissue engineering and remodeling due to the changing of the signaling pathway. Therefore, they conclude that a precise combination of micro-environmental stimuli may promote MSC differentiation [24].

In addition to the mechanical stimuli, many studies have shown the effect of electrical signals on the differentiation of different cell types such as Neural Precursor Cells (NPCs) [25–27]. Ariza et al. [25] report that NPCs differentiate into neurons but not into astrocytes or oligodendrocytes in the presence of a direct current Electric Field (dcEF). Moreover, Chang et al. [7,27] stated that exposing fetal NSCs to a particular magnitude of EF increases the ratios of neuronal cells, which is in agreement with other previous studies [25,26]. The study of Matos et al. [1] showed a marked peak in NSC viability under EFs and an enhanced tendency of astrocyte differentiation over neuronal differentiation under electric fields applied with a particular frequency. According to the results of Rajnicek et al. [28], the neurite growth in a weak dcEF depends on the contributions of the adhesivity and the net surface charge. They showed that the growth was oriented randomly on all the substrata in the absence of an EF. Other works have shown that whenever stationary cells are exposed to dcEFs, they reorient directionally [29,30] due to the imposed electrical and mechanical signals [31,32].

Among a wide range of biomaterials employed as cell ECM for *in vitro* investigations, hydrogels are considered as relevant alternatives. These are composed of water-swollen networks of cross-linked polymer chains which control their stiffness. Due to their nonlinear behavior, they can be altered by internal contractile forces exerted by cells or by other stretching and/or compressing forces [33,34].

Among other techniques [33,35,36], the local stiffness of hydrogels can be increased using remotely-induced internal forces which can be achieved by means of encapsulated magnetic nanoparticles that are embedded within the ECM and exposed to an external magnetic field [22]. Inducing an external magnetic field on these magnetic nanoparticles causes compression and/or traction of the hydrogel, leading to an increase in the bulk elastic modulus and consequently the hydrogel rigidity. To combine the electrotaxis effect with the previous mechanotactic influence, magnetic nanoparticles can be encapsulated within a piezoelectric matrix in such a way that an electrical field is generated due to the matrix deformation. In this way, to physically stimulate the piezoelectric material, encapsulating magnetic nanoparticles within the piezoelectric material makes it possible to remotely activate the piezoelectric material as well. Although the former method is helpful, the latter is more promising because it provides the possibility of increasing the bulk elastic modulus as well as the hydrogel rigidity while subjecting the cells to electrical signals [37,38]. Using this composite biocompatible material enables the generation of internal stimuli, introducing an electrical signal to the micro-environment, by applying mechanical solicitation without the need for any additional energy sources or electrodes [37–39]. Therefore, when an electroactive response is desired, piezoelectric materials may be a suitable novel alternative for active tissue engineering strategies.

Several numerical models have been developed to consider general patterns of tissue reconstruction resulting from external mechanical stimuli during fracture healing [40–47]. Although these models are helpful for predicting tissue repair, they consider neither the nonlinearity of the cell micro-environment nor cell differentiation and/or proliferation due to the mechanotactic and electrotactic process during

cell–ECM interaction. A numerical model considering cell differentiation and proliferation based on the mechanosensing process within a force-induced ECM with hyperelastic behavior has been previously presented by the authors [22]. The main objective of the present work is to extend the previously developed model to integrate the effect of the mechanotaxis with the electrotaxis using a piezoelectric material encapsulated along with magnetic nanoparticles. The aim of this combination is to study their effects on cell differentiation, migration, proliferation, and apoptosis when an internal force and an electrical field are remotely generated, via an external magnetic field, within the cell micro-environment.

2 Material and methods

In this work, the finite element is used to simulate the cell behavior within a nonlinear three-dimensional charged matrix with encapsulated piezoelectric spheres. The working domain is meshed using typical 3D solid hexahedral elements. The cell elements are forming a subdomain of the working domain in such a way that the elements of the working domain either belong to the ECM or to the cell (See Fig. 1). The cell morphology is kept constant during the calculations. This simplification allows the modeling of the complex cell behavior through the ECM without re-meshing difficulties (see [48] for more detail).

In the mechanosensing phase, the cell senses its ECM by exerting sensing forces at each cell membrane node to diagnose the rigidity of its surrounding ECM. As shown in Fig. 2a, these sensing forces are exerted on the nodes located on the cell surface, which belongs to the ECM too (cell-ECM interface). Hence, the cell-ECM interaction occurs by transferring the effect of cell nodal traction forces to the ECM conserving the displacement compatibility. In other words, the cell deforms itself using nodal traction forces on its membrane nodes so that the ECM becomes stressed and strained. Once the cell has determined its surrounding mechanical conditions, it starts to pull itself towards the stiffer and/or more fixed region by applying traction forces on the cell membrane nodes (See Fig. 2b). Hence, the cell centroid displaces according to cell polarization direction.

This model is developed under several fundamental assumptions:

1. The cell alignment due to mechanical signals is defined based on the direction of the minimum cell internal deformation which depends on the local changes of ECM stiffness and the imposed boundary conditions.
2. The concentration of the ligands at the leading edges of the cell is considered spatially uniform.
3. The cell has a constant 3D spherical shape.

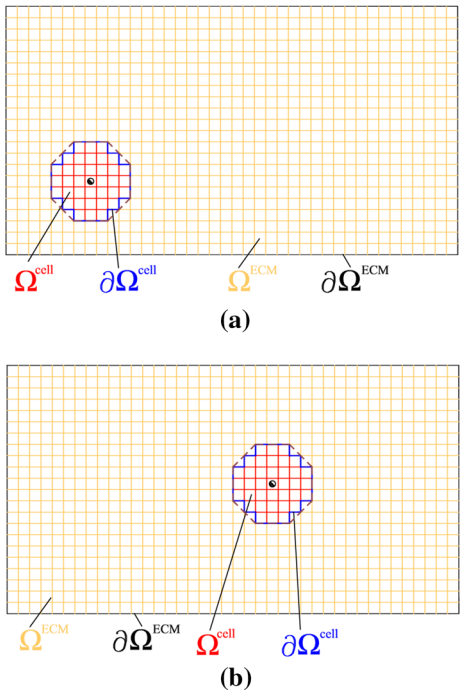

Fig. 1 2D schematic illustration of the cell and the ECM domains at step k **a** and step $k+1$ **b**. The cell domain is shown by Ω^{cell} with a boundary of $\partial\Omega^{cell}$ and ECM domain is shown by Ω^{ECM} with an external boundary of $\partial\Omega^{ECM}$, where $\Omega^{cell} \cup \Omega^{ECM}$ is the working domain. The ECM and cell in their interface have exactly matched nodes on $\partial\Omega^{cell}$. It is noteworthy that in the results, each cell is schematicaly visualized by a typical shell surface created using the cell nodes by means of "Delaunay Triangulation" (brown dash lines). (Color figure online)

4. During cell migration, differentiation, and proliferation, the cell volume is preserved.
5. The cell and its ECM material behavior are assumed to be nonlinear.
6. It is considered that there are neither thermal nor chemical active signals in the cell ECM.
7. There is no fluid flow in the ECM, considering it as continuum material.
8. There is no considerable degradation within the ECM.

2.1 ECM mechanical behavior

Here we consider that the ECM is composed of a hydrogel material which is frequently employed to investigate cell-ECM interaction [33,34]. Because these materials become stiffer when strained, the cell behavior can basically be changed when external or internal forces are applied in the ECM. As aforementioned, to control and modulate the cell differentiation, migration and proliferation it is possible to regulate the stiffening by means of remotely-induced internal forces in the cell micro-environment [49–51]. A neo-Hookean hyperelastic material model is here employed to

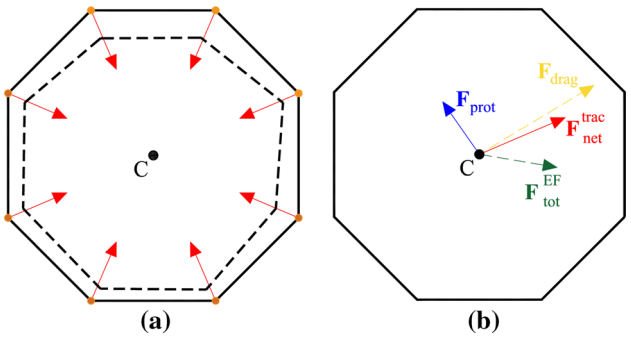

Fig. 2 **a** Cell deformation due to mechanosensing forces (red arrows) exerted on each node of the cell surface toward its centroid. **b** Effective forces on the cell during migration (net traction force, $\mathbf{F}_{\text{net}}^{\text{trac}}$, protrusion force, $\mathbf{F}_{\text{prot}}$, total electrostatic force, $\mathbf{F}_{\text{tot}}^{\text{EF}}$, and opposing drag force, $\mathbf{F}_{\text{drag}}$. (Color figure online)

properly predict the nonlinear behavior of such materials, covering a wide range of ECM stiffness ranging from a few to several hundred kPa [52]. Therefore, the strain energy function of the ECM for a relatively compressible material can be expressed by [53,54]

$$W_{\text{s}} = \frac{\mu}{2}\left(\overline{I}_1 - 3\right) + \kappa(J-1)^2 \tag{1}$$

where μ is a material constant with stress-like dimension and κ is the bulk modulus. $\overline{I}_1 = \text{tr}(\overline{\mathbf{C}})$ is the first invariant in terms of the right Cauchy-Green tensor, $\overline{\mathbf{C}} = \overline{\mathbf{F}}^{\text{T}}\overline{\mathbf{F}}$. $\overline{\mathbf{F}} = J^{1/3}\mathbf{F}$ is the purely isochoric contributions of the deformation gradient and $J = \det(\mathbf{F})$ is the Jacobian.

The Cauchy stress tensor can be obtained by the first derivation of the strain energy function and pushing forward as

$$\boldsymbol{\sigma}_{\text{s}} = \mu J^{-1}\left(\overline{\mathbf{B}} - \frac{1}{3}\overline{I}_1\mathbf{I}\right) + p\mathbf{I} \tag{2}$$

where $\overline{\mathbf{B}} = \overline{\mathbf{F}}\,\overline{\mathbf{F}}^{\text{T}}$ is the left Cauchy-Green tensor and $\mathbf{I}$ is the identity matrix. p is the hydrostatic pressure at a material point [55]. It can be defined as

$$p = 2\kappa(J-1) \tag{3}$$

2.2 Piezoelectric material behavior

Smart materials, generally known as active materials, are materials with reproducible, significant and stable variations of at least one property when subjected to external stimuli. A piezoelectric material is considered as a smart material that requires a certain anisotropy in its structure. Basically, it responds to any mechanical excitation such as stress or strain

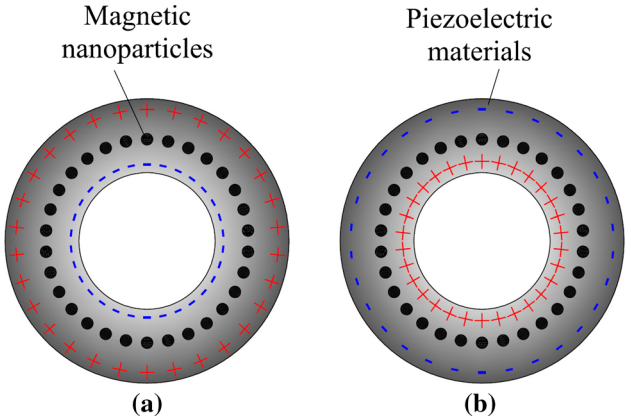

Fig. 3 Encapsulated magnetic nanoparticles together with a piezoelectric material. The external layer is the piezoelectric material along with the magnetic nanoparticles while the central core of the sphere is filled with the same material as the ECM. **a** Anodal side out, **b** cathodal side out

fields by generating an electrical potential gradient (and vice versa) [37,38].

To wisely control the response of the piezoelectric material embedded in the ECM, it can be encapsulated along with magnetic nanoparticles in a spherical shape of cell size in order to be stimulated by applying an external magnetic field. Using this technique, depending on the cultured cell type, it can be encapsulated in such a way that the anode or cathode be located on the outer surface (see Fig. 3). This piezoelectric sphere is embedded within the working domain and meshed by 3D solid hexahedral elements. It is connected through its external nodes with the ECM. The central core of the sphere is filled by a material of the same behavior as the surrounding ECM (Fig. 3).

The most relevant method to describe piezoelectric material behavior is the so-called direct effect, converting the mechanical energy (force induced by the nanoparticles) into electrical energy (electric potential gradient). This coupling between the electric potential gradient and the strain is the main property that governs the piezoelectric material's behavior. Therefore, assuming linear behavior, the constitutive equations that join the electrical potential gradient vector, $\mathbf{E}$, and the mechanical behavior of the piezoelectric material can be expressed by

$$\sigma_{ij}^{\text{pze}} = \mathbb{C}_{ijkl}\left(\epsilon_{kl}^{\text{pze}} - g_{mkl}q_m\right) \tag{4}$$

and

$$q_i = D_{im}g_{mjk}\sigma_{ij}^{\text{pze}} + D_{ij}E_j \tag{5}$$

where $\boldsymbol{\sigma}^{\text{pze}}$, $\boldsymbol{\epsilon}^{\text{pze}}$, $\mathbb{C}$, $\mathbf{q}$, $\mathbf{g}$ and $\mathbf{D}$ are the mechanical stress tensor, the strain tensor, the stiffness matrix defined at zero electrical potential gradient, the electric displacement vector,

the strain coefficient matrix of the piezoelectric material and the material's dielectric property, respectively [56].

2.3 Cell effective forces

2.3.1 Traction force

There are typically two main cellular elements that drive the cells. The first is the passive mechanical strength due to the resistance of cellular elements such as microtubules and the cell membrane, which is proportional to the passive cellular stiffness and the cell internal deformation. The second is the active cellular elements which generate contractile stress due to the overlap between actin filaments and myosin II that mainly depends on the minimum, ϵ_{min}, and the maximum, ϵ_{max}, internal strains of the cell. Therefore, approximating each cellular element with a linear elastic spring, the net cell stress transmitted to the ECM at each membrane node can be calculated as [22,57]

$$\sigma^{\text{cell}} = \begin{cases} & \epsilon^{\text{cell}} < \epsilon_{\min} \\ K_{\text{pas}}\epsilon^{\text{cell}} & \text{or} \\ & \epsilon^{\text{cell}} > \epsilon_{\max} \\ \frac{K_{\text{act}}\sigma_{\max}(\epsilon_{\min}-\epsilon^{\text{cell}})}{K_{\text{act}}\epsilon_{\min}-\sigma_{\max}} + K_{\text{pas}}\epsilon^{\text{cell}} & \epsilon_{\min} \le \epsilon^{\text{cell}} \le \tilde{\epsilon} \\ \frac{K_{\text{act}}\sigma_{\max}(\epsilon_{\max}-\epsilon^{\text{cell}})}{K_{\text{act}}\epsilon_{\max}-\sigma_{\max}} + K_{\text{pas}}\epsilon^{\text{cell}} & \tilde{\epsilon} \le \epsilon^{\text{cell}} \le \epsilon_{\max} \end{cases} \tag{6}$$

where K_{pas}, K_{act}, ϵ^{cell} and $\sigma_{\max}$ represent the stiffness of the passive and active cellular elements, the internal strain of the cell and the maximum contractile stress exerted by the actin-myosin machinery, respectively, while $\tilde{\epsilon} = \sigma_{\max}/K_{\text{act}}$.

The cell traction force, generated by contraction of the actin-myosin apparatus, is the main factor responsible for driving the cell forward in the direction of the minimum internal deformation (Maximum internal stress). It is proportional to the net stress transmitted by the cell to its ECM. Although the present model is applicable for any cell configuration [57,58], for the sake of simplicity a spherical cell configuration is here considered. This cell is represented by a connected group of finite elements, and the finite element methodology is used. So, the nodal traction force can be expressed as [48]

$$\mathbf{F}_i^{\text{trac}} = \sigma_i^{\text{cell}} S \zeta \mathbf{e}_i \tag{7}$$

where $\mathbf{e}_i$ stands for a unit vector passing from the cell centroid to the ith node of the cell membrane and S is the cell membrane area per node. The cell adhesivity ζ results from adhesivity sensed by the cell in its rear and front, which can be defined by

$$\zeta = k n_r \psi \tag{8}$$

where k, n_r and ψ represent the binding constant of the cell integrins, the total number of available receptors and the concentration of the ligands at the leading edge of the cell, respectively [48,59,60]. The net traction force acting on the whole cell membrane can be calculated as

$$\mathbf{F}_{\text{net}}^{\text{trac}} = \sum_{i=1}^{n} \mathbf{F}_i^{\text{trac}} \tag{9}$$

where n is the number of cell membrane nodes.

2.3.2 Generated force due to the electrical signal

The mechanisms by which electrical stimulation runs cellular migration and alters proliferation and differentiation are not yet fully understood. However, it is well known that the free calcium cations (Ca^{2+}) are the major factor in both direct and indirect mechanisms of electrotactic stimulation [29,30,61–65]. For instance, the role of cellular Ca^{2+} influx on electrotaxis has been observed in embryo mouse fibroblasts, neural crest cells, fish and human keratocytes [5,29,66–68]. However, no effect of cellular Ca^{2+} influx is observed in the electrotactic response of mouse fibroblasts [69].

In the resting state, a simple cell has a negative membrane potential [29]. Exposing a cell to EF leads the side of the plasma membrane that faces the cathode to be depolarized while the other side is hyperpolarized [5,29,67]. Thus, due to passive electrochemical diffusion, the hyperpolarized side of the membrane attracts Ca^{2+} leading to contraction and propelling the cell towards the cathode. This process continues until the voltage-gated Ca^{2+} channels (VGCCs) near the cathodal side are depolarized to allow Ca^{2+} influx (Fig. 4). Consequently, the resultant generated force will depend on the balance between the opposing magnetic contractile forces due to the increase of the intracellular Ca^{2+} level on both sides [29]. This is why some cells reorient towards the cathode, such as human keratinocytes [30,70], embryo fibroblasts [68], human retinal pigment epithelial cells [71] and fish epidermal cells [66], while others do so towards the anode, such as metastatic human breast cancer cells [72] and human granulocytes [73].

A cell which is located close enough to the piezoelectric material (which is charged due to forces exerted on magnetic nanoparticles) will be ionized and charged. Therefore, the force experienced by this individual charged cell can be obtained by

$$\mathbf{F}^{\text{EF}} = E \Omega S \mathbf{e}_{\text{EF}} \tag{10}$$

where E represents the magnitude of the electrical potential of the piezoelectric material in response to the compression or traction. Ω stands for the surface charge density of the cell

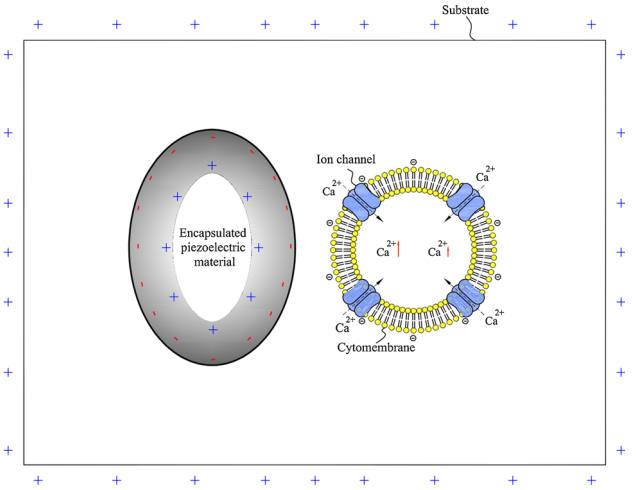

Fig. 4 Schematic illustration of the potential mechanism for the enhanced cellular response to an electrical signal. A simple cell in the resting state has a negative membrane potential [29]. When a cell with a negligible voltage-gated conductance is exposed to an electrical cue, its hyperpolarised membrane near the anode attracts Ca^{2+} due to passive electrochemical diffusion. Consequently, this side of the cell contracts, propelling the cell towards the cathode. Therefore, voltage-gated Ca^{2+} channels (VGCCs) near the cathode (depolarised side) open and Ca^{2+} influx occurs. In such a cell, the intracellular Ca^{2+} level rises on both sides. The direction of cell movement, then, depends on the difference between the opposing magnetic contractile forces which are exerted by the cathode and anode [29]

in the presence of the activated piezoelectric material. $\mathbf{e}_{EF}$ denotes a unit vector pointing from the cell centroid towards the centroid of the piezoelectric magnetic sphere.

The velocity of a cell exposed to an electrical signal strongly depends on the strength of the electrical potential generated by the piezoelectric material, in such a way that the higher the electrical potential generated by the piezoelectric sphere, the higher the cell surface charge density. Nishimura et al. [30] showed that the migration velocity of human keratinocytes is maximal when the electrical potential strength is about 100 mV/mm, decreasing with the reduction of the electrical potential magnitude. They stated that the increase of the electrical potential strength to 400 mV/mm has no effect on the net migration velocity of the cell. It seems that the electrical potential magnitude is correlated by increasing the concentration of the intracellular Ca^{2+}. Therefore, the surface charge of a cell is directly proportional to the magnitude of the imposed electrical potential [29,30]. Consequently, we assume a linear relationship between the cell surface charge and the electrical potential imposed by the piezoelectric material on the cell as

$$\Omega = \begin{cases} \frac{\Omega_{\text{satur}}}{E_{\text{satur}}} E & E \leq E_{\text{satur}} \\ \Omega_{\text{satur}} & E > E_{\text{satur}} \end{cases} \tag{11}$$

where Ω_{satur} is the saturation value of the surface charge and E_{satur} is the maximum electrical potential strength causing Ca^{2+} influx.

2.3.3 Drag force

The drag force is an opposing force that resists the cell motility [58,60]. The main objective here is to define a velocity-dependent opposing force associated with the viscous character of the ECM. For the sake of simplicity, we here assume a spherical cell configuration. However, the present model can be applied to any other cell configuration [57,58]. Referring to Stokes's drag regime, the drag force acting on a spherical cell can be presented by [48,60]

$$F_{\text{drag}} = 6\pi r \eta v \tag{12}$$

where r and v are the cell radius and velocity, respectively, while η is the effective viscosity of the medium. We assume that effective viscosity is linearly proportional to the medium stiffness, E_{ECM}, at each point. Therefore, we consider a bi-linear function to calculate effective viscosity through a medium with stiffness gradient as

$$\eta = \eta_{\min} + \lambda E_{\text{ECM}} \tag{13}$$

where $\eta_{\min}$ is the minimum viscosity of the ECM corresponding to minimum stiffness and λ is the proportionality coefficient. The viscosity coefficient may eventually be saturated with ECM rigidity [74].

2.3.4 Protrusion force

During migration, cells send out some local protrusions to probe their environment by exerting a random protrusion force. This force is generated by actin polymerization which is distinguished from the cytoskeletal contractile force [60]. This induces cells to move along a random path. Therefore, the direction and magnitude of the protrusion force are chosen randomly at each time step. It is worth noting that the order of magnitude of the protrusion force is the same as that of the traction force but with a lower amplitude [48,60,75]. So, it can be described as

$$\mathbf{F}_{\text{prot}} = \alpha F_{\text{net}}^{\text{trac}} \mathbf{e}_{\text{rand}} \tag{14}$$

where $\mathbf{e}_{\text{rand}}$ and α represent a random unit vector and a random scalar, $0 \leq \alpha < 1$, respectively, while $F_{\text{net}}^{\text{trac}}$ is the magnitude of the net traction force [32,48].

2.3.5 Cell–cell interaction

Cell–cell and cell–ECM interactions are controlling cell behavior during cell migration [76]. There is a direct relationship among the total cellular traction forces, cell–cell, and cell–ECM interactions [48,77]. It is indicated that the cell–cell generated tension is a fraction of the cell–ECM total traction force [76]. Thus, the variation of ECM properties influencing cell–ECM generated interaction forces, which in turn change cell–cell exerted contact forces [76]. Note that the cell exerts traction forces through its integrins on the ECM or on the neighbor cells. The exerted contact force between two cells in contact can be determined by the calculation of the resultant of the nodal traction forces of their common nodes (for instance, the summation of the exerted nodal traction forces of the nodes n_1, n_2, n_3, and n_4 in Fig. 5). Therefore, in the present model, cell–cell contact forces are automatically included within the force equilibrium of each cell (Eq. 9) through the nodal traction forces (Eq. 7) of their nodes in contact.

In this work, during the mechanosensing process, we assume that when two or more cells come into contact with each other (see Fig. 5), their sides (nodal points) in common are not able to send out any pseudopods to sense the ECM [48,78,79]. Therefore, these cells do not exert any sensing force at those nodes until they are separated again. Note that even though there is no sensing force in the nodes that are in contact, the corresponding deformation and consequently the nodal traction forces are not zero (see Eqs. 6, 7). This is because all the cell nodes, including the nodes that are in contact (n_1, n_2, n_3, and n_4 in Fig. 5), deform together due to deformation compatibility. More details can be found in [31,48]. To avoid interference of two cells we assume

$$\| \mathbf{r}_j - \mathbf{r}_i \| \geq 2r \tag{15}$$

where $\mathbf{r}_i$ and $\mathbf{r}_j$ are the position vector of each cell centroid (Fig. 5).

Furthermore, in the presence of an electrical signal, cells face a cell–cell electrostatic force due to cell charge. Therefore, the electrostatic force generated between the ith and jth cells, $\mathbf{F}_{ij}^{EF}$, can be expressed as

$$\mathbf{F}_{ij}^{\mathrm{EF}} = \frac{k_{\mathrm{e}}}{\epsilon_{\mathrm{r}}} \left(\frac{\Omega S}{\| \mathbf{r}_{ij} \|} \right)^2 \mathbf{e}_{ij} \tag{16}$$

where k_{e} is the Coulomb's constant in the vacuum and $\mathbf{r}_{ij}$ is the vector joining the centroids of these two cells (Fig. 5). ϵ_{r} is the relative permittivity (dielectric constant) of the medium and, finally, $\mathbf{e}_{ij}$ is the direction of the force generated between the two cells. It is known that due to the electrostatic charge and for one cell type in the same ECM, cells tend to repel each other. So that

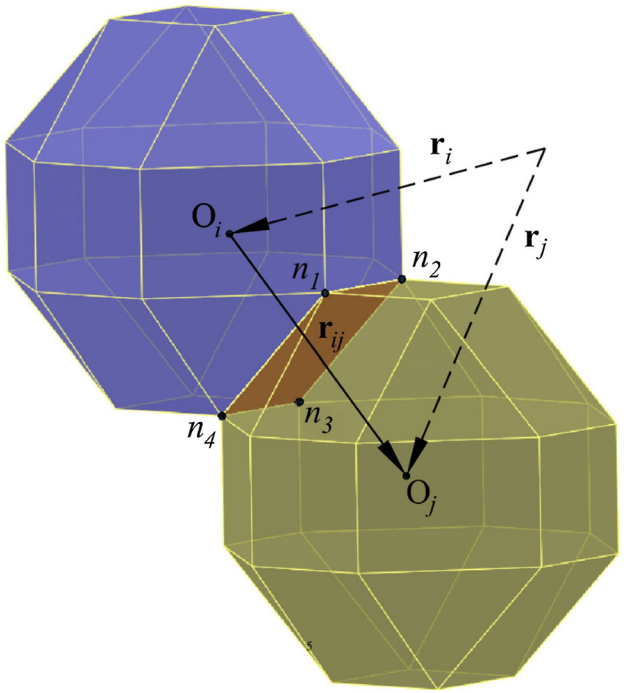

Fig. 5 Position vector and distance between the centroids of two cells in contact

$$\mathbf{e}_{ij} = -\frac{\mathbf{r}_{ij}}{\| \mathbf{r}_{ij} \|} \tag{17}$$

Therefore, the resultant electrostatic force exerted by a cell population on the ith cell can be calculated as

$$\mathbf{F}_{ip}^{\mathrm{EF}} = \sum_{j=1}^{n_c - 1} \mathbf{F}_{ij}^{\mathrm{EF}} \tag{18}$$

where n_c is the number of cells. Consequently, the net electrostatic force acting on a cell in the presence of a piezoelectric sphere can be calculated as

$$\mathbf{F}_{\mathrm{tot}}^{\mathrm{EF}} = \mathbf{F}^{\mathrm{EF}} + \mathbf{F}_{ip}^{\mathrm{EF}} \tag{19}$$

At the microscale (the dimension of the cell and its ECM is here in microscale), the viscous resistance dominates the inertial resistance of the cell due to its negligible mass [48, 60], so that the force balance (See Fig. 2b) can be represented by

$$\mathbf{F}_{\mathrm{net}}^{\mathrm{trac}} + \mathbf{F}_{\mathrm{tot}}^{\mathrm{EF}} + \mathbf{F}_{\mathrm{prot}} = \mathbf{F}_{\mathrm{drag}} \tag{20}$$

2.4 Mechanosensing and cell reorientation

Following experimental observations [14,80], we consider that, in the mechanosensing phase, the cell exerts sensing

forces at each finite element node of the cell membrane towards the corresponding cell centroid to assess its microenvironment. Therefore, the finite element analysis of the working domain delivers deformation of the working domain in Gauss points level in consequence of these sensing forces. The nodal deformation of each node of the working domain, including the ith node of the cell membrane, can be calculated by the projection of the deformation from Gauss points to the element nodes. So, the cell internal strain at the ith finite element node of its membrane can be expressed as

$$\epsilon_i^{\text{cell}} = \mathbf{e}_i : \boldsymbol{\epsilon}_i : \mathbf{e}_i^{\text{T}} \tag{21}$$

where $\boldsymbol{\epsilon}_i$ represents the strain tensor of the ith node during the mechanosensing process. Subsequently, during time step, τ, the translocation vector of the cell through which the cell migrates to a new position can be defined from Eqs. 12 and 20 as

$$\mathbf{d} = \frac{\tau}{6\pi r\eta}\left(\mathbf{F}_{\text{net}}^{\text{trac}} + \mathbf{F}_{\text{tot}}^{\text{EF}} + \mathbf{F}_{\text{prot}}\right) \tag{22}$$

2.5 Cell differentiation, proliferation and apoptosis

Cells may respond to the mechanical characteristics of their ECM, such as ECM stiffness, by differentiation, proliferation and/or apoptosis [8–11]. Many experimental investigations have shown that a cell undergoes a specific differentiation when it senses a particular deformation [23,41,81]. The reason is that a cell can recognize which ECM resembles its original tissue from different points of view such as the ECM rigidity and the magnitude and duration of the received mechanical and/or electrical signals. In addition, large deformations may cause cell apoptosis if they exceed a threshold up to which a typical cell can endure [8,10].

We consider here that MSCs are susceptible to differentiating into a specific cell type $i \in \{l, c, s\}$, where l, c and s represent neuroblast, chondrocyt and osteoblast lineage specifications, respectively. It is considered that internal deformation of the cell in the polarization direction induces mechano-regulation of the cell differentiation. Internal deformation in the cell polarization direction, which varies temporally and spatially [41,43,82], can be calculated by

$$\gamma(\mathbf{x}, t) = \mathbf{e}_{pol} : \sum_{i=1}^{n} \boldsymbol{\epsilon}_i : \mathbf{e}_{pol}^{\text{T}} \tag{23}$$

where $\mathbf{e}_{pol} = \frac{\mathbf{d}}{\|\mathbf{d}\|}$ denotes the cell polarization direction.

Moreover, many experimental observations indicate that cells such as MSCs [83] and chondrocytes [84] require a certain minimal time to become sufficiently mature to undergo differentiation and/or proliferation, indicating time dependency of the cell differentiation and proliferation. This means that the cell needs a time period to be active in the differentiation and/or proliferation stage [43,83–85]. Because, in this work, the cell shape and volume are preserved, it can be assumed that, before cell differentiation, the growth, if any, occurs during maturation time. Therefore, cell differentiation and proliferation processes are also here related to a cell maturation time which can be moderated by the mechanical signals received by a typical cell depending on the cell type. Stronger mechanical signals increase the differentiation or proliferation rate, decreasing the cell maturation time. However, even within hydrogels that produce the strongest mechanical signals, cells require a minimum time period to initiate differentiation and/or proliferation processes [85]. Hence, we here assume that the cell maturation time is linearly proportional to the cell internal deformation as

$$t_{\text{mat}}(\gamma, t) = t_{\text{min}} + t_{\text{p}}\gamma(\mathbf{x}, t) \tag{24}$$

where t_{min} is the least time needed for a typical cell to start differentiation or proliferation and t_{p} is a time proportionality. Therefore, besides the lineage specifications $i \in \{m, l, c, s\}$ (m denotes the MSC phenotype), each cell type is also represented by a Maturation Index (MI) described as [86]

$$\text{MI} = \begin{cases} \frac{t}{t_{\text{mat}}} & t \le t_{\text{mat}} \\ 1 & t > t_{\text{mat}} \end{cases} \tag{25}$$

A fully mature cell carries MI = 1, meaning that it is ready for differentiation or proliferation if the appropriate mechanical stimulus is received, while MI = 0 represents a very young cell, meaning that it is not yet able to differentiate or proliferate even if it receives the appropriate mechanical signal. The evolution of cell maturation is assumed to be an irreversible process, indicating that the MI cannot decrease over time. Considering these conditions, the MSC differentiation and apoptosis process can be linked to maturation and mechanical stimuli by [22,43]

$$\text{Cell phenotype} = \begin{cases} s & \gamma_{\text{l}} < \gamma \le \gamma_s \ \&\ \text{MI} = 1 \\ c & \gamma_s < \gamma \le \gamma_c \ \&\ \text{MI} = 1 \\ l & \gamma_c < \gamma \le \gamma_{\text{u}} \ \&\ \text{MI} = 1 \\ \text{apoptosis} & \gamma_{\text{apop}} < \gamma \\ \text{no differentiation} & \text{otherwise} \end{cases} \tag{26}$$

where γ_{u} and γ_{l} represent upper and lower bounds of cell internal deformations, respectively. γ_{s} and γ_{c} denote the maximum cell internal deformation that stimulates the MSC to differentiate into osteoblasts and chondrocytes, respectively.

During the cell proliferation process, two daughter cells are generated from a single mother cell. Four different steps

are considered in this process, comprising the first growth phase (G1), the synthesis phase (S), the second growth phase (G2) and the mitosis phase (M), respectively [87,88]. During the G1 phase, the cell synthesizes biological material in order to grow while in the S phase it replicates the sister chromatids. The G2 phase is to proofread and to ensure that the DNA is appropriately replicated before cell division in the M phase during which a mother cell is divided into two daughter cells. However, after the M phase some cells may participate in the cell proliferation cycle while other cells temporarily stop proliferation, entering into the quiescence state (G0) [87,88].

To model the proliferation process in a biologically consistent way, we consider the dominant phases of the cell division in such a way that the cell proliferation cycle is split into two main steps: during the G1, S and G2 phases the cell grows and matures; and when it receives a mechanical signal it enters into the M phase where one mature mother cell is divided into two non-mature daughter cells. Consequently, in the present model, we assume that a cell is either in the maturation stage or in the proliferation phase as [22,86]

$$\text{Cell growth} = \begin{cases} \text{cell division} & \gamma \leq \gamma_i^{\text{prof}} \ \& \ \text{MI} = 1 \\ \text{no cell division} & \text{otherwise} \end{cases} \tag{27}$$

where $i \in \{m, l, c, s\}$ and $\gamma_i^{\text{prof}} < \gamma_{\text{u}}$ is the maximum cell internal deformation which can cause the proliferation of cell i [43]. After division, we assume that one of the daughter cells is located in the mother cell location, $\mathbf{x}_{\text{daut}}^{(1)} = \mathbf{x}_{\text{moth}}$, while the other is located in its neighborhood as $\mathbf{x}_{\text{daut}}^{(2)} = \mathbf{x}_{\text{moth}} + 2r\mathbf{e}_{\text{rand}}$. The "daut" and "moth" subscripts represent daughter and mother cells, respectively.

3 Finite element implementation

The present model is implemented in the commercial Finite Element (FE) software ABAQUS [89] through a coupled user-defined element (UEL) [32,90,91] and is solved using Abaqus implicit scheme in which the backward Euler time integration is used to discretize the system of equations. Note that the backward scheme should be employed with precaution because it may not conserve the angular momentum in many situations [92,93], which is not our case. The corresponding flowchart is presented in Fig. 6. Using different degrees of stiffness, several numerical examples are here studied to demonstrate the application of the present model in the prediction of cell differentiation and proliferation within a Force-Induced Substrate using a Piezoelectric material (FIS-PZE). The results presented here are compared with those relating to a Force-Free Substrate (FFS) and a Force-Induced Substrate using a Rigid body (FIS-R) previously published by the same authors [22]. The ECM dimensions are here assumed to be $1000 \times 500 \times 500$ μm, where a cell is located far from the ECM boundaries to discard the effect of the boundary conditions on the cell behavior. Basically, the cell initial location will not affect the final results whereas the cell tends to migrate towards the piezoelectric sphere located in the working domain due to mechano- and electro-sensing. However, if the cell is located far from the piezoelectric sphere, at the first instance of the cell differentiation or proliferation may be delayed. The working domain, including the cell and its ECM, is meshed structurally by 128,000 linear 3D hexahedral elements and 136,161 nodes. The outer layer of the piezoelectric sphere embedded in the working domain is meshed by linear 3D hexahedral electrical elements with ten layers of elements in the radial direction while the internal core is meshed by linear 3D hexahedral elements. The cell is assumed to have a spherical shape ($\phi 32$ μm) and, at each time step, different 48 elements from working domain are assigned to the cell. Piezoelectric dielectric constant in the direction of piezoelectric material thickness is assumed 1.3×10^{-12}. It is considered that magnetic nanoparticles are encapsulated within a piezoelectric matrix with the same dimensions as that of the cell and a thickness of a half of its radius, while it is embedded in the center of the cell's ECM. To combine the electrotaxis and mechanotactic effects, an external magnetic field is induced on magnetic nanoparticles encapsulated within the piezoelectric matrix. This causes compression and/or traction of the hydrogel and, consequently, leads to an increase in the bulk elastic modulus of the hydrogel. Besides, due to the generated force, the piezoelectric matrix will become deformed and charged. Assuming that the outer surface of the piezoelectric matrix is the cathode (anode), depending on the application and cell type, it is considered that the whole cell's ECM is surrounded by the anode (cathode). Consequently, an electric field gradient from all directions towards the ECM center is generated which activates the electrotactic stimuli to the cell. The calculation time is about one minute for each time step, corresponding to approximately 6 h of real cell-ECM interaction [86]. Table 1 shows the properties of the ECM, the cell and the piezoelectric material. Although in the presented model it is possible to assign different elastic modulus for the cell and ECM, for simplicity, we assume that the cell has the same elastic modulus of its ECM. This is consistent with the fact that elasticity of the adhering cells can be tuned to approximate that of its tissues [94]. The feedback of local matrix stiffness on cell state has important implications for development, differentiation, proliferation and regeneration [95].

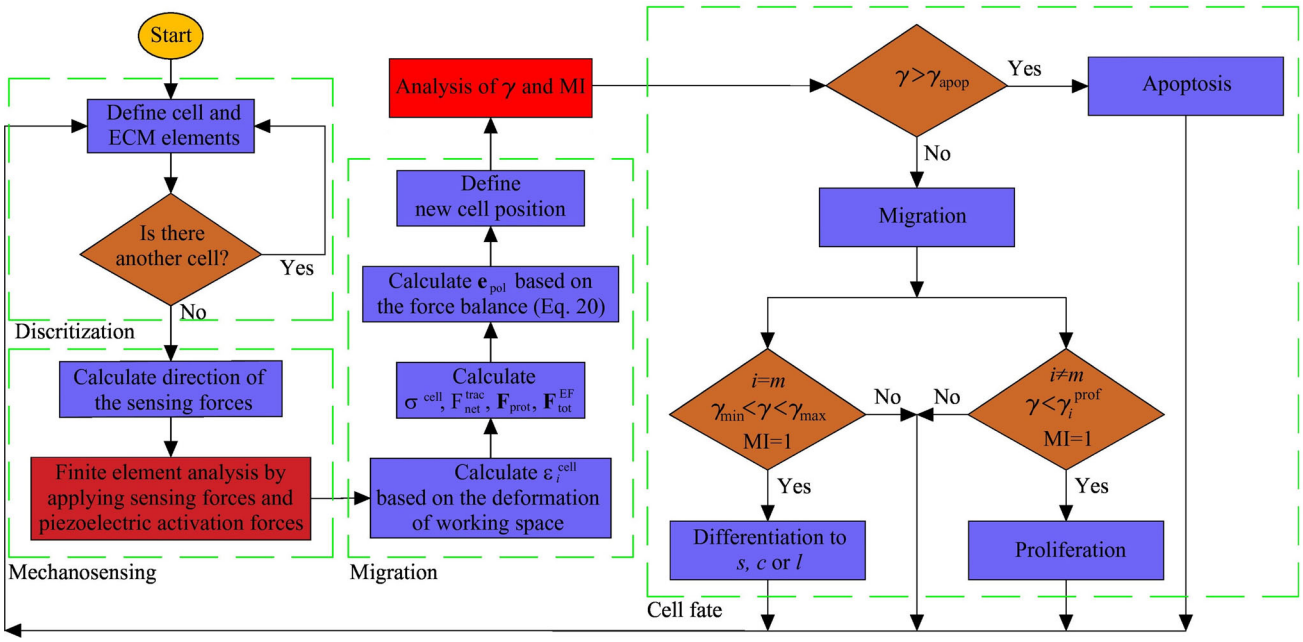

Fig. 6 Flowchart of the numerical implementation of the model including cell mechanosensing, migration, and consequent cell fate decision due to mechanotaxis and electrotaxis. Note that γ_{min} and γ_{max} correspond to the consistent γ_u and γ_l, γ_s, and γ_c according to Eq. 26 and Table 1

Table 1 General parameters employed in the model except where other values are specified

Symbol	Description	Value	References
η_{min}	ECM viscosity	1000 Pa s	[60,96]
λ	Proportionality coefficient	0.4 μm min	[74]
K_{pas}	Stiffness of microtubules	2.8 kPa	[97]
K_{act}	Stiffness of myosin II	2 kPa	[97]
ϵ_{max}	Maximum strain of the cell	0.9	[48,98]
ϵ_{min}	Minimum strain of the cell	−0.9	[48,98]
σ_{max}	Maximum contractile stress exerted by actin-myosin machinery	0.1 kPa	[99,100]
$k_f = k_b$	Binding constant at rear and front of the cell	10^8 mol^{-1}	[60]
n_{r_f}	Number of available receptors at the front of the cell	1.5×10^5	[60]
n_{r_b}	Number of available receptors at the back of the cell	10^5	[60]
ψ	Concentration of the ligands at rear and front of the cell	10^{-5} mol	[60]
t_{min}	Minimum time needed for cell proliferation	4 days	[43,85]
t_p	Time proportionality	200 days	[43,85]
γ_l	Lower bound of cell internal deformation leading to osteoblast differentiation	0.005	[43,101]
γ_s	Upper bound of cell internal deformation leading to osteoblast differentiation	0.04	[43,101]
γ_c	Upper bound of cell internal deformation leading to chondrocyte differentiation	0.1	[43]
γ_u	Upper bound of cell internal deformation leading to neuroblast differentiation	0.5	[22]
γ_{apop}	Cell internal deformation leading to cell apoptosis	1	[43]
γ_i^{prof}	Limit of cell proliferation	0.2	[43]
g	Piezoelectric coefficient in the direction of piezoelectric material thickness	1.0 pC/N	[38]

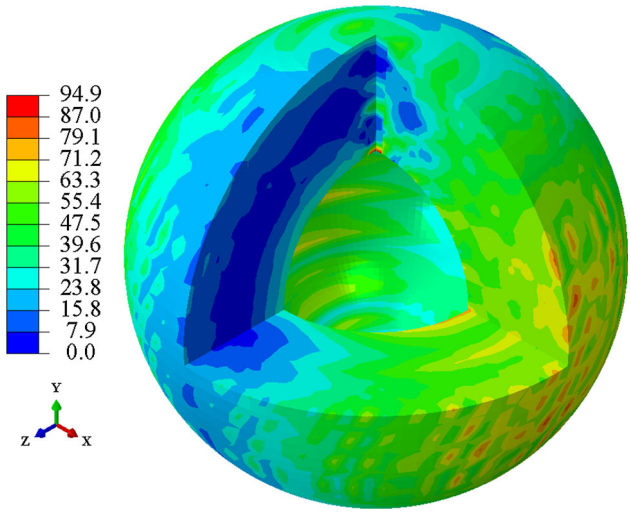

Fig. 7 A section of the piezoelectric sphere embedded within the cell's ECM after its stimulation by an external magnetic force. The color distribution showing the distribution of the electrical potential gradient (mV/mm) (see also V1 Video). Note that the magnetic force is exerted in the longitudinal x-direction. (Color figure online)

4 Results

4.1 Electrical signal generated by piezoelectric matrix

Many recent investigations have demonstrated the effectivity of the electric field in controlling cell behavior in many cases such as wound healing where it accelerates the healing process [4]. For instance, electrical potential gradients ranging between 0 and 140 mV/mm have been measured at the wound edge, proving that even small electric fields applied to cell micro-environments can control the behavior of different cell types inducing them to migrate directionally [4].

Here, it is assumed that the hydrogel is induced by a magnetic force in the longitudinal direction (x-direction) to stimulate the piezoelectric matrix which in turn generates an electric field. It is worth noting that the generated magnetic force increases the ECM rigidity as shown and discussed in [22]. This increment of the ECM rigidity, as shown in our previous work [22], increases the osteogenic ECM stiffness to the upper value of the corresponding stiffness bound ($\sim$ 44.6 kPa). For this case, a 5 μN traction force is needed to apply to the magnetic nanoparticles. This force generates a maximum electrical potential gradient of $\sim$ 94.9 mV/mm, as seen in Fig. 7.

4.2 MSC proliferation and differentiation within an osteogenic-like FIS-PZE

Initially, we designed a numerical example to consider both the MSC proliferation and differentiation within an osteogenic-like FIS-PZE. It is compared with the corresponding numerical example of MSC proliferation and differentiation within osteogenic-like FFS and FIS-R previously published by the same authors [22]. At the beginning, the ECM stiffness is equal to 30 kPa (the lower bound of osteogenic-like ECM) [102] while applying force on the piezoelectric matrix locally increases it to $\sim$ 45 kPa (the upper bound of osteogenic-like ECM). Both the MSC proliferation and differentiation are permitted through this example. As the MSC maturates within the osteogenic-like FIS-PZE, one mature mother MSC proliferates and delivers two immature daughter cells after $\sim$ 8 days, as seen in Fig. 8a. Depending on the mechanical signal received by the new daughter cells, γ, they may undergo differentiation or proliferation after maturation. Here, the first MSC differentiation into osteoblast occurs after $\sim$ 25.25 days (Fig. 8b) and the process can be followed after each cell maturation by either MSC proliferation and differentiation or by osteoblast proliferation (Fig. 8c). In Table 2, the obtained results are summarized. Likewise, as in the previous works by the same authors [22,86], in the instance of MSC differentiation and proliferation, there is a sudden jump in the average net traction force (results are not shown here), which is qualitatively consistent with the experimental work of Fu et al. [103]. Zemel et al. [104] suggest that this can be attributed to the changes in the quality of the cell adhesion to its ECM in consequence of the MSC differentiation. However, in the case of cell proliferation, the reason may be the asymmetric distribution of the internal cell deformation due to cell–cell interaction [86,91]. It is worth noting that in the presence of electrotaxis the cells keep moving around the piezoelectric matrix located in the ECM center. Therefore, due to the strong signal (less internal deformation) received by the cells, they experience a lower maturation time and consequently the cell proliferation rate increases and MSC differentiation advances in comparison with the cell proliferation and differentiation within osteogenic-like FFS and FIS-R, as shown in [22].

4.3 MSC lineage specification within an osteogenic-like FIS-PZE

This numerical example is prepared in order to investigate the fate decision of MSCs within an osteogenic-like FIS-PZE. The results here are shown from the moment of MSC differentiation to avoid repeating the representation of the MSC proliferation. At the beginning, the ECM stiffness is equal to 30 kPa and locally increased to $\sim$ 45 kPa by exerting an internal force (5 μN) on the piezoelectric matrix in the longitudinal direction (x-direction), as occurred in the presence of the rigid body in the previous study [22]. Moreover, an electrical potential gradient is generated by the piezoelectric matrix, generating an electrical signal in the middle of the cell's ECM. The MSC is gradually maturated during cell-

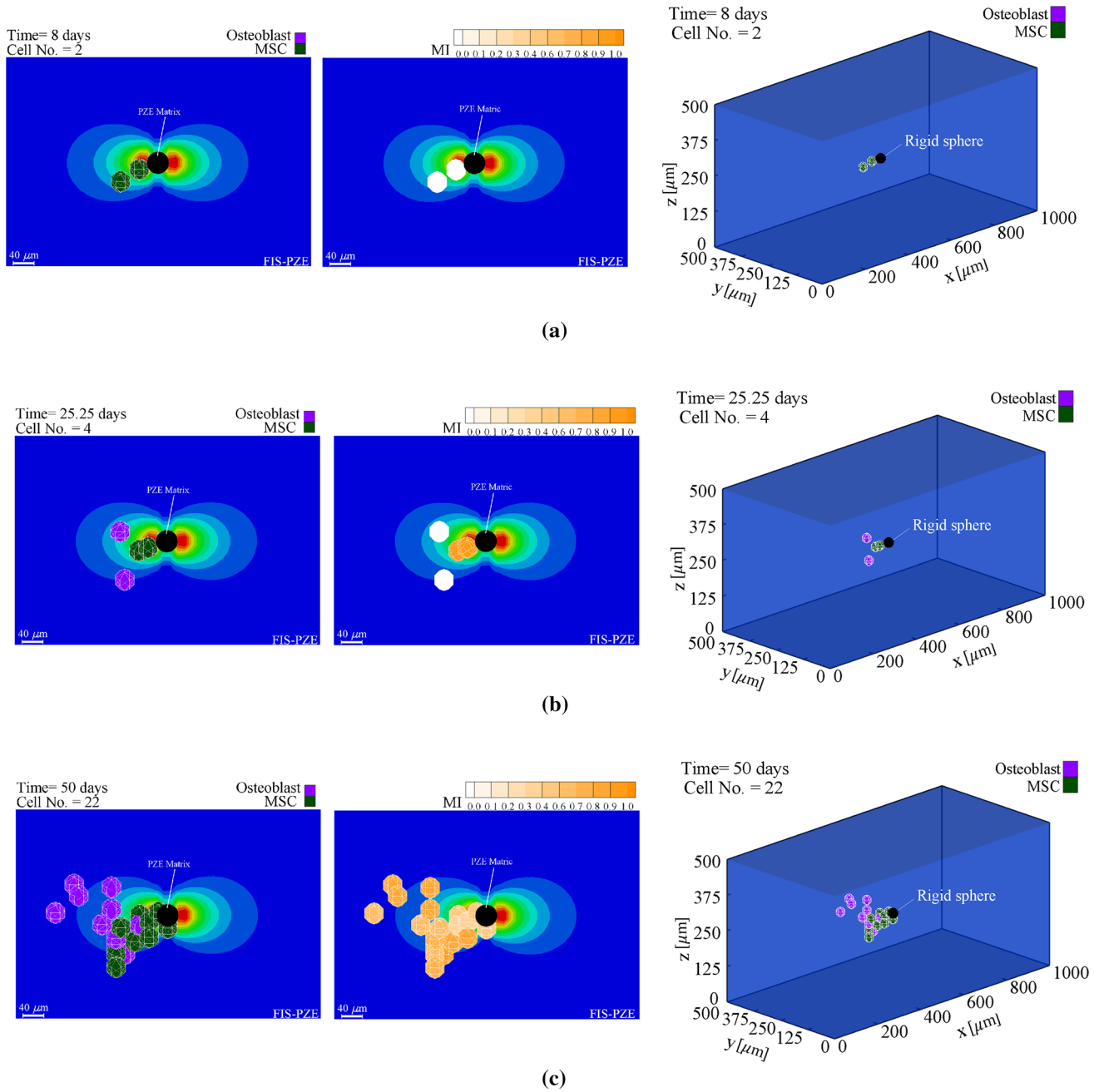

Fig. 8 MSCs proliferation and differentiation within an osteogenic-like FIS-PZE. **a** The initial moment of MSC proliferation, **b** the initial moment of MSC differentiation into osteoblast and **c** the continuation of MSC differentiation and proliferation of MSCs and osteoblasts (see also V2 Video). Note that the color gradient in the background from blue to red corresponds to the minimum (30 KPa) and the maximum (45 KPa) bounds of the ECM stiffness, respectively. (Color figure online)

Table 2 Summary of the obtained results

ECM type	Elapsed time to start MSC differentiation (days)	Elapsed time to start cell proliferation (days)	No. of cells at the end of the simulation
Osteogenic-like FIS-PZE	5.25	11	99
Chondrogenic-like FIS-PZE	7.25	15.25	31
Neurogenic-like FIS-PZE	12.5	25.75	19

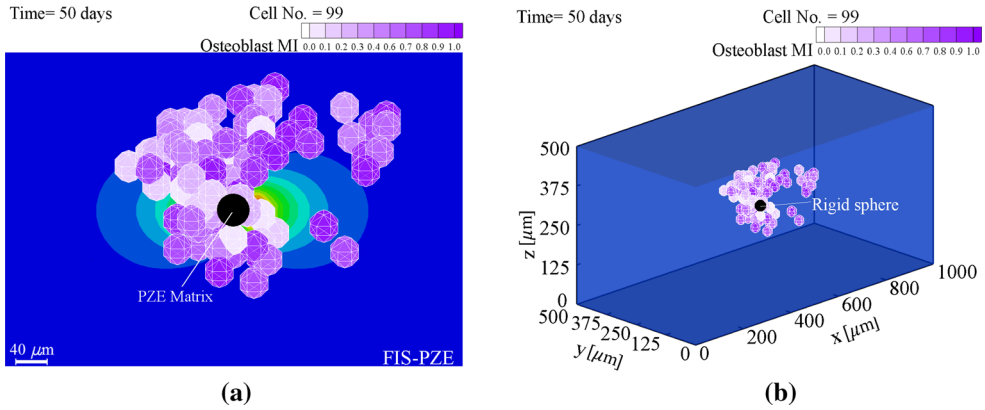

Fig. 9 Osteoblast proliferation within an osteogenic-like FIS-PZE (see also V3 Video). Note that the color gradient in the background from blue to red corresponds to the minimum (30 KPa) and the maximum (45 KPa) bounds of the ECM stiffness, respectively

ECM interaction and then differentiates into osteoblast when it is fully mature (MI = 1) after ∼ 5.25 days. Experimental findings [12,18,105] also confirm MSC differentiation to osteoblast within ECM resembling osteogenic tissues. Each new maturated osteoblast may continue proliferation when it senses the appropriate mechanical signal. After ∼ 50 days, an osteoblast which is differentiated from a single MSC proliferates into 99 osteoblasts, as seen in Fig. 9. Comparing the MSC lineage specification within the osteogenic-like FIS-PZE (Fig. 9) with those specifications previously published by the same authors [22], it can be deduced that MSC differentiation and osteoblast proliferation within the osteogenic-like FIS-PZE is much faster than those of FFS and FIS-R. This can also be noted by comparing the density of osteoblasts within different ECM in Fig. 10. This is due to the presence of electrotaxis in the cell micro-environment that guides the cells more directionally towards the ECM center and leads to the decrease in the cell maturation time because the cells feel less deformation, γ, in the stiffer regions such as the ECM center (see also Fig. 11). The acceleration of MSC differentiation into osteoblast within force-induced ECM has been observed experimentally [23,24]. Moreover, directional cell movement in the presence of electrotaxis towards the source of the electrical signal has been observed in many experimental [3,4,29,30,63] and numerical [31,32,57] works. These explain further why the rate of osteoblast proliferation increases and MSC differentiation advances within an osteogenic-like FIS-PZE in comparison with those of FFS and FIS-R [22]. In addition, note that, as shown in a previous work by the same authors [86], MSC differentiation into osteoblast as well as osteoblast proliferation lead to a sudden increase in the average magnitude of the net traction force [31] (results are not shown here), which is in agreement with the experimental findings of Fu et al. [103].

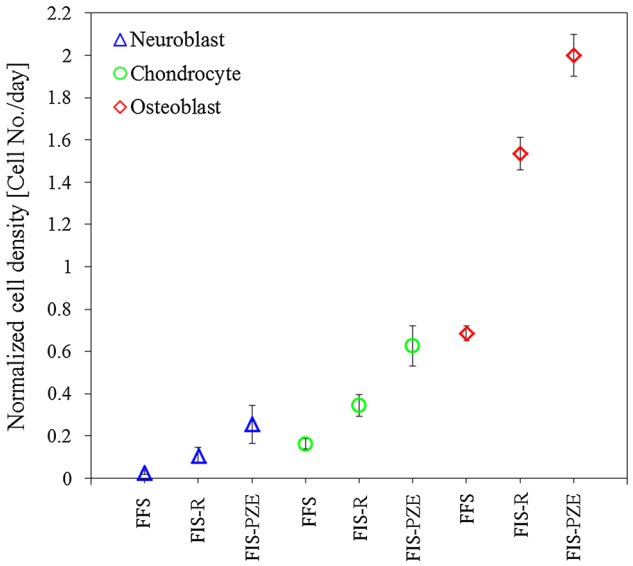

Fig. 10 Normalized density of each cell phenotype in FFS [22], FIS-R [22] and FIS-PZE during identical times in consequence of MSC differentiation and proliferation. The error bars represent mean standard deviation of different runs. (Color figure online)

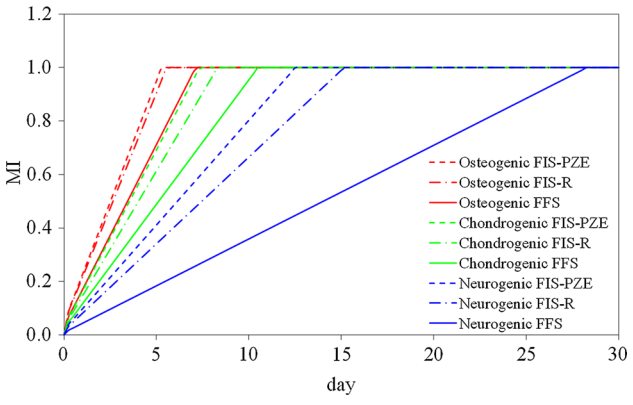

Fig. 11 MI of MSCs within ECM with different characteristics

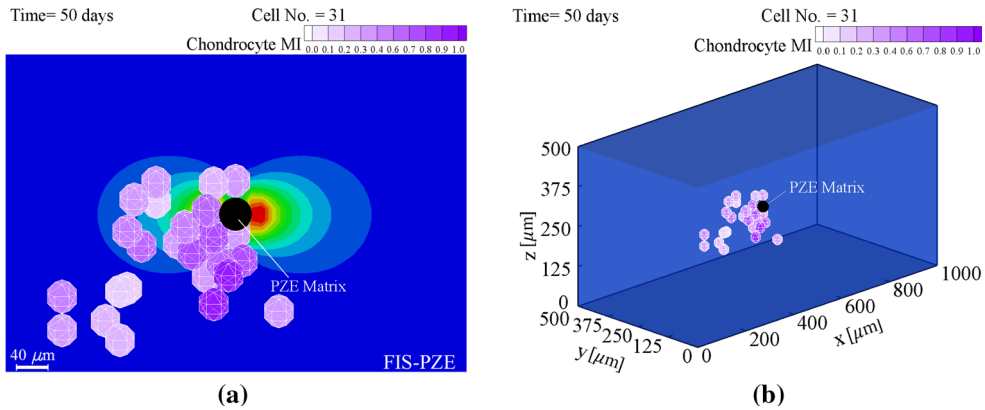

Fig. 12 Chondrocyte proliferation within a chondrogenic-like FIS-PZE (see also V4 Video). Note that the color gradient in the background from blue to red corresponds to the minimum (20 KPa) and the maximum (25 KPa) bounds of the ECM stiffness, respectively. (Color figure online)

4.4 MSC lineage specification within a chondrogenic-like FIS-PZE

This numerical example is designed to study the lineage specification of MSCs within chondrogenic-like FIS-PZE. Again, to concentrate only on the results of the chondrocyte proliferation, the results are shown from the instance of MSC differentiation. At the beginning, the cell's ECM stiffness is set to 20 kPa (the lower bound of chondrogenic tissue stiffness) [102] while force inducement in the longitudinal direction locally increases the ECM stiffness up to $\sim$ 25 kPa (the upper bound of chondrogenic tissue stiffness). An electrical potential gradient is generated by the piezoelectric matrix. A MSC is located around the piezoelectric matrix and gradually matures during the cell-ECM interaction. A completely mature MSC differentiates into chondrocyte after $\sim$ 7.25 days. Subsequently, given the appropriate mechanical signal, the proliferation process continues through maturation of the new chondrocyte and after $\sim$ 50 days 31 chondrocytes are generated as seen in Fig. 12. Figures 10 and 12 indicate that the density of chondrocytes within the chondrogenic-like FIS-PZE is greater than that of chondrocytes within chondrogenic-like FFS and FIS-R (see also Fig. 8a, b of the previously published work by the same authors [22]). The progression of the differentiation and proliferation processes within the chondrogenic-like FIS-PZE is consistent with the experimental findings of Kurpinski et al. [23,24], which is attributed to the decrease in the cell maturation time because of the increase in the ECM rigidity [106]. In the case of a chondrogenic-like FIS-PZE, the electrical signals in addition to the force inducement accelerate the cell proliferation and differentiation because hey help the cells to keep moving sufficiently close to ECM center, where cells can sense stronger mechanical signals (lower internal deformation) and consequently need less maturation time, as can be seen in Fig. 11. As in the previous example, in this case there is also a jump in the magnitude of the net traction force at the instance of the MSC differentiation, consistent with the observations of Fu et al. [103]. Besides, the average magnitude of the net traction force increases after chondrocyte proliferation due to associated cell–cell interaction (results are not shown here).

4.5 MSC lineage specification within a neurogenic-like FIS-PZE

We have designed this numerical example to consider the lineage specification of MSCs within a neurogenic-like FIS-PZE. Following the previous numerical examples, we focus on the results starting from the moment of MSC differentiation. Initially, a MSC is located close to the piezoelectric matrix within the neurogenic-like FIS-PZE with a stiffness of 0.1 kPa (the lower bound of neurogenic tissue) [102]. Due to applying a force on the piezoelectric matrix in the longitudinal direction (x-direction), in addition to increasing the ECM stiffness to about 1 kPa (the upper bound of neurogenic tissue), an electrical signal is generated in the cell's micro-environment. A maturated MSC differentiates into neuroblast after $\sim$ 12.5 days within a neurogenic-like FIS-PZE. Afterwards, a neuroblast continues the proliferation process and generates 19 chondrocytes after $\sim$ 75 days, as seen in Fig. 13. Note that maturation the time decreases within a neurogenic-like FIS-PZE (Fig. 11) and that the differentiation and proliferation processes occur quicker than within both a neurogenic-like FFS and FIS-R (compare Fig. 13 with Fig. 9a, b of the previous work by the same authors [22]). Therefore, the cell density within a neurogenic-like FIS-PZE is higher in comparison with that of a neurogenic-like FFS and a FIS-R, as seen in Fig. 10. As mentioned before, this is because, in addition to the increase in ECM rigidity, an electrical signal exists in the cell microenvironment which advances the instant of cell maturation by keeping cells around the piezoelectric matrix in the ECM center. In the case of adipoblasts, Fu et al. [103] previously

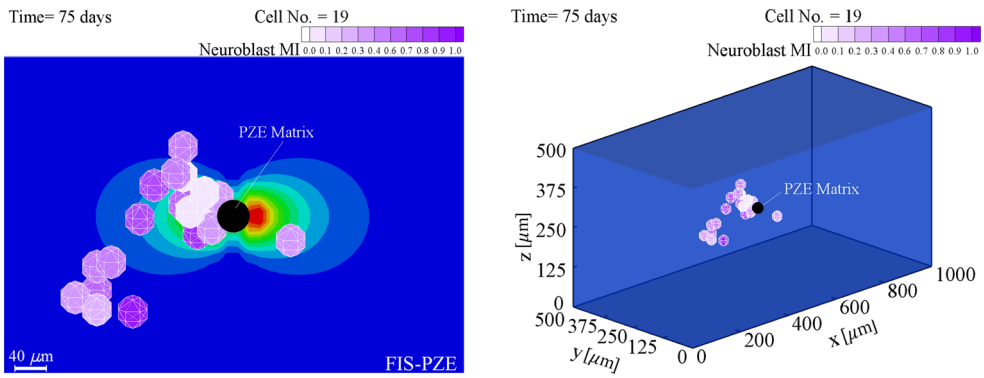

Fig. 13 Neuroblast proliferation within a force-induced neurogenic-like ECM and in the presence of the electrical signal generated by a piezoelectric matrix (see also V5 Video). Note that the color gradient in the background from blue to red corresponds to the minimum (0.1 KPa) and the maximum (1 KPa) bounds of the ECM stiffness, respectively. (Color figure online)

observed the advancement of MSC differentiation due to an increase in the relatively soft ECM. It is worth noting that the magnitude of the net traction force decreases due to MSC differentiation into neuroblast, consistent with previous experimental [103] and numerical [86] works. It seems that MSCs are more contractile within a neurogenic-like ECM in comparison with neuroblasts. In this case, as in the previous cases, the cell–cell interaction increases the average magnitude of the net traction force due to neuroblast proliferation (data not presented here).

5 Discussion

5.1 General remarks and comments

In addition to chemical and thermal inducers, other physical cues, including mechanical and electrical, can guide cell fate and proliferation [107]. As discussed above, the self-renewal characteristics of MSCs provide them with significant potential to undergo lineage specification, such as osteoblast, chondrocyte and neuroblast. Recent advances towards achieving a better understanding of the mechanisms and signaling pathways that regulate the lineage specification of MSCs have provided new insights into their potential for clinical applications, particularly for tissue repair and regeneration [3,4,12,19,23,24,29,30,63]. Moreover, experimental observations have proved that MSC differentiation and proliferation can be controlled remotely either by regulating the mechanical properties of the cellular micro-environment via an internal force or by stimulating the cell to migrate directionally by means of electrotaxis towards stiffer regions [4,12,19]. Many studies [19,41] have proposed different hypotheses to reveal how mechanical signals may control cell lineage specifications. However, the accurate mechanical pathway by which the cell micro-environment regulates the cell differentiation and proliferation is still not fully understood.

Recently, a 3D FE model was developed by the same authors to investigate the effects of ECM stiffness on cell lineage specification within FFS and FIS-R [22,86]. Here the previous model is extended to study the effect of electrotaxis on cell differentiation and proliferation within an ECM with controlled stiffness. To the best of our knowledge, this is the first study that has investigated the behavior of MSCs within an ECM with controlled stiffness using an internal force in the presence of electrotaxis generated by means of piezoelectric material.

The present nonlinear model is here employed to interpret cell response and fate when its ECM is induced by an internal force along with the presence of an electrical cue. In this work, it is shown how cell fate can be dictated by controlling ECM stiffness in the presence of electrotaxis due to force inducement on the magnetic nanoparticles encapsulated along with piezoelectric material. The results for FIS-PZE are compared with previously presented results for FFS and FIS-R by the same authors. Our findings indicate that considering different ECM stiffness bounds, the presence of electrotaxis increases the rate of cell proliferation and advances MSC differentiation. This occurs because the electrical signal forces the cell to remain in stiffer regions in the ECM where encapsulated piezoelectric material is located. This is qualitatively in agreement with previous experimental observations which indicate that, for a typical cell, cell internal deformation transferred by focal adhesions of integrins plays a key role in the mechanosensing process [12,18,23,24,103–105]. Consistent with experimental works [23,108], a local increase in the ECM stiffness decreases the cell internal deformation and, in turn, accelerates the cell proliferation and differentiation. This can be achieved by

inducing internal forces within the ECM. Maintaining the cell within these stiffer regions can be established by introducing local electrostatic signals in these regions via encapsulated piezoelectric material. This reveals the reason why the cell differentiation advancement and proliferation rate increase when its ECM is stimulated by an internal force [24,105].

Our findings indicate that the cell maturation time significantly affects the cell differentiation or proliferation (in agreement with experimental observations [109]). Therefore, cells might become fully mature faster and differentiate/proliferate quicker within FIS-PZE than within FIS-R or FFS (see Fig. 11). At the moment of MSC differentiation, the net traction force generated by a typical cell may suddenly increase (osteoblasts and chondrocytes) or decrease (neuroblast), which is consistent with experimental observation [103] and our previous numerical work [22,86]. The reason may be the better alignment of the cell stress fibers due to the compatibility of the ECM and the cell stiffness at the moment of the MSC differentiation. Besides, cell–cell interaction leads to an asymmetric distribution of the traction force on the cell membrane, causing a considerable increase in the average net traction force of a typical cell at the moment of proliferation (discussed in [31]).

5.2 Effect of the model parameters

Here, various parameters and constants are used and pre-adjusted during each simulation. It is important to choose these parameters wisely and consistent with cell type to achieve the appropriate cell destination within its corresponding ECM.

Recently developed biomaterials enable us to create 3D ECMs with tunable material parameters. Cells seeded within this 3D medium can migrate based on the ECM stiffness, architecture, and even pore size [110]. It is an advantage for a model to have the capability of capturing a wide variety of behaviors when proper model parameters are chosen. All parameters used here are selected from well-known numerical or experimental literature (Table 1). The actin stiffness, K_{act}, is one of the sensitive parameters because it directly affects the net cell stress, σ^{cell}, and consequently the nodal traction forces, $\mathbf{F}_i^{\text{trac}}$. Therefore, changing the actin stiffness can directly change the cell velocity, maturation time and differentiation and proliferation rates. It is noteworthy that, keeping other parameters constant in the model, the cell velocity has a peak at the ECM stiffness of ~ 45 kPa (results are not shown), causing an increase of the traction forces until saturation. Consequently, the lower values of actin stiffness are, the slower cell migration towards ECM regions with higher rigidity is and, in turn, the lower cell proliferation and differentiation rates are. This comes from lower actin-myosin overlap which decreases contraction forces and leads to higher forces.

On the other hand, we benefit prior works [43,85,101] to define γ_{u}, γ_{l}, γ_{s}, γ_{c}, t_{p} and t_{min}. Therefore, one should take precaution when he uses the presented model. For instance, if the range of the cell internal deformations is inappropriately defined, it may lead to physically wrong cell lineage specification. So, the recommended technique is to obtain these parameters experimentally from the ECM, in which the cells are aimed to be cultured.

5.3 Effect of mesh size

To employ this model, one must select the mesh size wisely whereas it can increase quickly the computational cost. Therefore, one must find a balance in between the accuracy of the results and the needed computational time.

In the present work, at each time step, the cell displacement is calculated and accumulated to the previous one. Therefore, until the cell displacement is not big enough (for example, if it is less than the length of one element) to move the cell central element to another neighbor element (one of the 24 existing neighboring elements), the cell elements remain unchanged. Therefore, the cell will keep its position until the accumulated calculated displacement is equal to or more than one element size. At this moment, it will move to the next element. So, the effect of the element size will be mainly in the cell movement visualization. In a coarse mesh, the cell will be seen in a discrete movement while in the case of fine mesh, the cell movement will be smoother. However, if one is looking for the incremental trajectory of the cell centroid from one time step to another, which is our case, the mesh size has a tiny effect if it is selected wisely.

6 Conclusions

To conclude, we believe that the local increase of the ECM stiffness by internal forces and maintaining the cell translocation around stiffer regions by an electrotactic cue can be considered an outstanding technique for remotely controlling the cell response and may open a new door in tissue regeneration methodologies. Besides, the present 3D numerical model can successfully predict essential aspects of cell maturation, differentiation, proliferation, and apoptosis within nonlinear ECMs. However, further studies of different mechanical and physical factors such as cell shape, chemical signals, and colony size are required for a deeper understanding of the mechanisms behind the cell lineage specification.

Acknowledgements The authors gratefully acknowledge the financial support from the Spanish Ministry of Economy and Competitiveness (MINECO MAT2016-76039-C4-4-R, AEI/FEDER, UE), the Government of Aragon (DGA-T24_17R) and the Biomedical Research Networking Center in Bioengineering, Biomaterials and Nanomedicine

(CIBER-BBN). CIBER-BBN is financed by the Instituto de Salud Carlos III with assistance from the European Regional Development Fund.

References

1. Matos MA, Cicerone MT (2010) Alternating current electric field effects on neural stem cell viability and differentiation. Biotechnol Prog 26(3):664–70
2. Clause KC, Liu LJ, Tobita K (2010) Directed stem cell differentiation: the role of physical forces. Cell Commun Adhes 17(2):48–54
3. Maria EM, Djamgoz MBA (2004) Cellular mechanisms of direct-current electric field effects: galvanotaxis and metastatic disease. J Cell Sci 117(Pt 9):1631–39
4. Zhao M (2009) Electrical fields in wound healing-an overriding signal that directs cell migration. Semin Cell Dev Biol 20(6):674–82
5. Gao RC, Zhang XD, Sun YH, Kamimura Y, Mogilner A, Devreotes PN, Zhao M (2011) Different roles of membrane potentials in electrotaxis and chemotaxis of dictyostelium cells. Eukaryot Cell. https://doi.org/10.1128/EC.05066-11
6. Zhao H, Steiger A, Nohner M, Ye H (2015) Specific intensity direct current (DC) electric field improves neural stem cell migration and enhances differentiation towards βIII-tubulin+ neurons. PLoS One 10(6):e0129625
7. Chang HF, Lee YS, Tang TK, Cheng JY (2016) Pulsed dc electric field-induced differentiation of cortical neural precursor cells. PLoS ONE 11(6):e0158133
8. Kearney EM, Prendergast PJ, Campbell VA (2008) Mechanisms of strain-mediated mesenchymal stem cell apoptosis. J Biomech Eng 130(6):061004
9. Harrison NC, del Corral RD, Vasiev B (2011) Coordination of cell differentiation and migration in mathematical models of caudal embryonic axis extension. PLoS ONE 6(7):e22700
10. Gladman SJ, Ward RE, Michael-Titus AT, Knight MM, Priestley JV (2010) The effect of mechanical strain or hypoxia on cell death in subpopulations of rat dorsal root ganglion neurons in vitro. Neuroscience 171:577–87
11. Ulrich TA, De Juan Pardo EM, Kumar S (2009) The mechanical rigidity of the extracellular matrix regulates the structure, motility, and proliferation of glioma cells. Cancer Res 69(10):4167–4174
12. Engler AJ, Sen S, Sweeney HL, Discher DE (2006) Matrix elasticity directs stem cell lineage specification. Cell 126(4):677–89
13. Aubry D, Gupta M, Ladoux B, Allena R (2015) Mechanical link between durotaxis, cell polarity and anisotropy during cell migration. Phys Biol 12(2):026008
14. Lo CM, Wang HB, Dembo M, Wang YL (2000) Cell movement is guided by the rigidity of the substrate. Biophys J 79(1):144–152
15. Lee DA, Knight MM, Campbell JJ, Bader DL (2011) Stem cell mechanobiology. J Cell Biochem 112(1):1–9
16. Lee Y, Huang J, Wangc Y, Lin K (2013) Three-dimensional fibroblast morphology on compliant substrates of controlled negative curvature. Integr Biol 5(12):1447–55
17. Maul TM, Chew DW, Nieponice A, Vorp DA (2011) Mechanical stimuli differentially control stem cell behavior: morphology, proliferation, and differentiation. Biomech Model Mechanobiol 10(6):939–53
18. Huebsch N, Arany PR, Mao AS, Shvartsman D, Ali OA, Bencherif SA, Rivera-Feliciano J, Mooney DJ (2010) Harnessing traction-mediated manipulation of the cell/matrix interface to control stem-cell fate. Nat Mater 9:518–26
19. Li D, Zhou J, Chowdhury F, Cheng J, Wang N, Wang F (2011) Role of mechanical factors in fate decisions of stem cells. Regen Med 6(2):229–40
20. Palomares KT, Gleason RE, Mason ZD, Cullinane DM, Einhorn TA, Gerstenfeld LC, Morgan EF (2009) Mechanical stimulation alters tissue differentiation and molecular expression during bone healing. J Orthop Res 27(9):1123–32
21. Marklein RA, Burdick JA (2010) Spatially controlled hydrogel mechanics to modulate stem cell interactions. Soft Matter 6:136–143
22. Mousavi SJ, Doweidar MH (2016) Numerical modeling of cell differentiation and proliferation in force-induced substrates via encapsulated magnetic nanoparticles. Comput Methods Prog Biomed 130:106–17
23. Kurpinski K, Chu J, Hashi C, Li S (2006) Anisotropic mechanosensing by mesenchymal stem cells. Proc Natl Acad Sci USA 103(44):16095–100
24. Kurpinski K, Chu J, Wang D, Li S (2009) Proteomic profiling of mesenchymal stem cell responses to mechanical strain and TGF-β1. Cell Mol Bioeng 2(4):606–14
25. Ariza CA, Fleury AT, Tormos CJ, Petruk V, Chawla S, Oh J et al (2010) The influence of electric fields on hippocampal neural progenitor cells. Stem Cell Rev 6:585–600
26. Lim JH, McCullen SD, Piedrahita JA, Loboa EG, Olby NJ (2013) Alternating current electric fields of varying frequencies: effects on proliferation and differentiation of porcine neural progenitor cells. Cell Reprogr 15:405–12
27. Chang KA, Kim JW, Kim JA, Lee SE, Kim S, Suh WH et al (2011) Biphasic electrical currents stimulation promotes both proliferation and differentiation of fetal neural stem cells. PLoS ONE 6:e18738
28. Rajnicek AM, Robinson KR, McCaig CD (1998) The direction of neurite growth in a weak dc electric field depends on the substratum: contributions of adhesivity and net surface charge. Dev Biol 203(2):412–23
29. Mycielska ME, Djamgoz MB (2004) Cellular mechanisms of directcurrent electric field effects: galvanotaxis and metastatic disease. J Cell Sci 117(9):1631–1639
30. Nishimura KY, Isseroff RR, Nuccitelli R (1996) Human keratinocytes migrate to the negative pole in direct current electric fields comparable to those measured in mammalian wounds. J Cell Sci 109(1):199–207
31. Mousavi SJ, Doblaré M, Doweidar MH (2014) Computational modelling of multi-cell migration in a multi-signalling substrate. Phys Biol 11(2):026002 (17 pp)
32. Mousavi SJ, Doweidar MH, Doblaré M (2013) 3D computational modelling of cell migration: a mechano-chemo-thermo-electrotaxis approach. J Theor Biol 329:64–73
33. Ahearne M (2014) Introduction to cell-hydrogel mechanosensing. Interface Focus 4:20130038
34. Ahearne M, Wilson SL, Liu KK, Rauz S, El Haj AJ, Yang Y (2010) Influence of cell and collagen concentration on the cell-matrix mechanical relationship in a corneal stroma wound healing model. Exp Eye Res 91:584–591
35. Ahearne M, Yang Y, Then KY, Liu KK (2008) Nondestructive mechanical characterisation of UVA/riboflavin crosslinked collagen hydrogels. Br J Ophthalmol 92:268–271
36. Brown RA, Wiseman M, Chuo CB, Cheema U, Nazhat SN (2005) Ultrarapid engineering of biomimetic materials and tissues: fabrication of nano- and microstructures by plastic compression. Adv Funct Mater 15:1762–70
37. Ribeiro C, Correia DM, Ribeiro S, Sencadas V, Botelho G, Lanceros-Méndez S (2015) Piezoelectric poly(vinylidene fluoride) microstructure and poling state in active tissue engineering. Eng Life Sci 15:351–6
38. Ribeiro C, Sencadas V, Correia DM, Lanceros-Méndez S (2015) Piezoelectric polymers as biomaterials for tissue engineering applications. Colloids Surf B Biointerfaces 136:46–55

39. Lovinger AJ (1982) Developments in semicrystalline polymers. Elsevier, London
40. Carter DR, Blenman PR, Beaupré GS (1988) Correlations between mechanical stress history and tissue differentiation in initial fracture healing. J Orthop Res 7:398–407
41. Claes LE, Heigele CA (1999) Magnitudes of local stress and strain along bony surfaces predict the coarse and type of fracture healing. J Biomech 32:255–66
42. Geris L, van Oosterwyck H, Vander Sloten J, Duyck J, Naert I (2003) Assessment of mechanobiological models for the numerical simulation of tissue differentiation around immediately loaded implants. Comput Methods Biomech Biomed Eng 6:277–88
43. Kang KT, Park JH, Kim HJ, Lee HM, Lee K-I, Jung HH, Lee HY, Shim YB, Jang JW (2011) Study on differentiation of mesenchymal stem cells by mechanical stimuli and an algorithm for bone fracture healing. Tissue Eng Reg Med 8(4):359–70
44. Kelly DJ, Prendergast PJ (2005) Mechano-regulation of stem cell differentiation and tissue regeneration in osteochondral defects. J Biomech 38(7):1413–22
45. Lacroix D, Prendergast PJ (2002) A mechano-regulation model for tissue differentiation during fracture healing: analysis of gap size and loading. J Biomech 35:1163–71
46. Lacroix D, Prendergast PJ, Li G, Marsh D (2002) Biomechanical model of simulate tissue differentiation and bone regeneration: application to fracture healing. Med Biol Eng Comput 40:14–21
47. Stops AJ, Heraty KB, Browne M, O'Brien FJ, McHugh PE (2010) A prediction of cell differentiation and proliferation within a collagen-glycosaminoglycan scaffold subjected to mechanical strain and perfusive fluid flow. J Biomech 43(4):618–26
48. Mousavi SJ, Doweidar MH, Doblaré M (2012) Computational modelling and analysis of mechanical conditions on cell locomotion and cell-cell interaction. Comput Methods Biomech Biomed Eng. https://doi.org/10.1080/10255842.2012.710841
49. Jha AK, Jackson WM, Healy KE (2014) Controlling osteogenic stem cell differentiation via soft bioinspired hydrogels. PLoS ONE 9(6):e98640
50. Nagaoka S, Tanzawa H, Suzuki J (1990) Cell proliferation on hydrogels. Vitro Cell Dev Biol 26(1):51–6
51. Wang T, Sun W, Liu X, Wang C, Fu S, Tong Z (2013) Promoted cell proliferation and mechanical relaxation of nanocomposite hydrogels prepared in cell culture medium. React Funct Polym 73(5):683–9
52. Sanabria-DeLong N, Crosby AJ, Tew GN (2008) Photocrosslinked PLA-PEO-PLA hydrogels from self-assembled physical networks: mechanical properties and influence of assumed constitutive relationships. Biomacromolecules 9(10):2784–91
53. Mousavi SJ, Avril S (2017) Patient-specific stress analyses in the ascending thoracic aorta using a finite-element implementation of the constrained mixture theory. Biomech Model Mechanobiol. https://doi.org/10.1007/s10237-017-0918-2
54. Ogden RW (1998) Nonlinear elastic deformations. Dover, New York
55. Mousavi SJ, Farzaneh S, Avril S (2017) Computational predictions of damage propagation preceding dissection of ascending thoracic aortic aneurysms. Int J Numer Method Biomed Eng. https://doi.org/10.1002/cnm.2944
56. Allik H, Hughes TJR (1970) Finite element method for piezoelectric vibration. Int J Numer Methods Eng 2(2):151–7
57. Mousavi SJ, Doweidar MH (2015) Three-dimensional numerical model of cell morphology during migration in multi-signaling substrates. PLoS ONE 10(3):e0122094
58. Mousavi SJ, Doweidar MH (2014) A novel mechanotactic 3D modeling of cell morphology. J Phys Biol 11(4):046005
59. Schwarz US, Balaban NQ, Riveline D, Bershadsky A, Geiger B, Safran SA (2002) Calculation of forces at focal adhesions from elastic substrate data: the effect of localized force and the need for regularization. Biophysics 83(3):1380–94
60. Zaman MH, Kamm RD, Matsudaira P, Lauffenburgery DA (2005) Computational model for cell migration in three-dimensional matrices. Biophys J 89:1389–1397
61. Armon L, Eisenbach M (2011) Behavioral mechanism during human sperm chemotaxis: involvement of hyperactivation. PLoS ONE 6:e28359
62. Hong CB, Fontana DR, Poff KL (1983) Thermotaxis of dictyostelium discoideum amoebae and its possible role in pseudoplasmodial thermotaxis. Proc Natl Acad Sci USA 80:5646–49
63. Long H, Yang G, Wang Z (2011) Galvanotactic migration of ea.hy926 endothelial cells in a novel designed electric field bioreactor. Cell Biochem Biophys 61:481–91
64. Rajabi AH, Jaffe M, Arinzeh TL (2015) Piezoelectric materials for tissue regeneration: a review. Acta Biomater 24:12–23
65. Shanley LJ, Walczysko P, Bain M, MacEwan DJ, Zhao M (2006) Influx of extracellular Ca^{2+} is necessary for electrotaxis in dictyostelium. J Cell Sci 119:4741–48
66. Cooper MS, Shliwa M (1986) Motility of cultured fish epidermal cells in the presence and absence of direct current electric fields. J Cell Biol 102:1384–1399
67. Nuccitelli R (2003) A role for endogenous electric fields in wound healing. Curr Top Dev Biol 58:1–26
68. Onuma EK, Hui SW (1985) A calcium requirement for electric field-induced cell shape changes and preferential orientation. Cell Calcium 6:281–292
69. Brown MJ, Loew LM (1994) Electric field-directed fibroblast locomotion involves cell surface molecular reorganization and is calcium independent. J Cell Biol 127:117–128
70. Sheridan DM, Isseroff RR, Nuccitelli R (1996) Imposition of a physiologic dc electric field alters the migratory response of human keratinocytes on extracellular matrix molecules. J Invest Dermatol 106:642–646
71. Sulik GL, Soong HK, Chang PC, Parkinson WC, Elner SG, Elner VM (1992) Effects of steady electric fields on human retinal pigment epithelial cell orientation and migration in culture. Acta Ophthalmol (Copenh.) 70:115–122
72. Fraser SP, Diss JKJ, Mycielska ME, Coombes RC, Djamgoz MBA (2002) Voltage-gated sodium channel expression in human breast cancer: possible functional role in metastasis. Breast Cancer Res Treat 76:S142
73. Rapp B, Boisfleury-Chevance A, Gruler H (1988) Galvanotaxis of human granulocytes. dose–response curve. Eur Biophys J 16:313–319
74. Dokukina IV, Gracheva ME (2010) A model of fibroblast motility on substrates with different rigidities. Biophys J 98:2794–803
75. James DW, Taylor JF (1969) The stress developed by sheets of chick fibroblasts in vitro. Exp Cell Res 54:107–110
76. Maruthamuthu V, Sabass B, Schwarz US, Gardel ML (2011) Cell-ECM traction force modulates endogenous tension at cell–cell contacts. Proc Natl Acad Sci USA 108(12):4708–13
77. Palsson E (2001) A three-dimensional model of cell movement in multicellular systems. Future Gener Comput Syst 17:835–852
78. Brofland GW, Wiebe CJ (2004) Mechanical effects of cell anisotropy on epithelia. Comput Methods Biomech Biomed Eng 7(2):91–99
79. Taylor DL, Heiple J, Wang YL, Luna EJ, Tanasugarn L, Brier J, Swanson J, Fechheimer M, Amato P, Rockwel M, Daley G (1982) Cellular and molecular aspects of amoeboid movement. CSH Symp Quant Biol 46:101–111
80. Trichet L et al (2012) Evidence of a large-scale mechanosensing mechanism for cellular adaptation to substrate stiffness. Proc Natl Acad Sci 109(18):6933–38

81. Wozniak MA, Chen CS (2009) Mechanotransduction in development: a growing role for contractility. Nat Rev Mol Cel Biol 10:34–43
82. Prokharaua PA, Vermolena FJ, Garcia-Aznar JM (2014) A mathematical model for cell differentiation, as an evolutionary and regulated process. Comput Methods Biomech Biomed Eng 17(10):1051–70
83. Delaine-Smith RM, Gwendolen CR (2012) Mesenchymal stem cell responses to mechanical stimuli. Muscles Ligaments Tendons J 2(3):169–80
84. Wu QQ, Chen Q (2000) Mechanoregulation of chondrocyte proliferation, maturation, and hypertrophy: ion-channel dependent transduction of matrix deformation signals. Exp Cell Res 256(2):383–91
85. Cullinane DM, Salisbury KT, Alkhiary Y, Eisenberg S (2003) Effects of the local mechanical environment on vertebrate tissue differentiation during repair: does repair recapitulate development. J Exp Biol 206:2459–71
86. Mousavi SJ, Doweidar MH (2015) Role of mechanical cues in cell differentiation and proliferation: a 3d numerical model. PLoS ONE 10(5):e0124529
87. Fouliarda S, Benhamidaa S, Lenuzzab N, Xaviera F (2009) Modeling and simulation of cell populations interaction. Math Comput Model 49(11):2104–8
88. Théry M, Bornens M (2006) Cell shape and cell division. Curr Opin Cell Biol 18(6):648–57
89. Hibbit D, Karlson B, Sorensen P (2011) Abaqus-theory manual, 6.11-3 edn. Hibbitt, Karlsson & Sorensen, Inc., Pawtucket, RI
90. Farzaneh S, Paseta O, Gómez-Benito MJ (2015) Multi-scale finite element model of growth plate damage during the development of slipped capital femoral epiphysis. Biomech Model Mechanobiol 14(2):371–85
91. Mousavi SJ, Doweidar MH, Doblaré M (2013) Cell migration and cell–cell interaction in the presence of mechano-chemo-thermotaxis. Mol Cell Biomech 10(1):1–25
92. Simo JC, Tarnow N (1992) The discrete energy-momentum method. Conserving algorithms for nonlinear elastodynamics. ZAMP 43(5):757–92
93. Campello EMB, Pimenta PM, Wriggers P (2011) An exact conserving algorithm for nonlinear dynamics with rotational DOFs and general hyperelasticity. Part 2: shells. Comput Mech 48(2):195–211
94. Solon J, Levental I, Sengupta K, Georges PC, Janmey PA (2007) Fibroblast adaptation and stiffness matching to soft elastic substrates. Biophys J 93(12):4453–61
95. Discher DE, Janmey P, Wang YL (2005) Tissue cells feel and respond to the stiffness of their substrate. Science 310(5751):1139–43
96. Akiyama SK, Yamada KM (1985) The interaction of plasma fibronectin with fibroblastic cells in suspension. J Biol Chem 260(7):4492–4500
97. SchÃd'fer A, Radmacher M (2005) Influence of myosin ii activity on stiffness of fibroblast cells. Acta Biomater 1:273–280
98. Ramtani S (2004) Mechanical modelling of cell/ECM and cell/cell interactions during the contraction of a fibroblast-populated collagen microsphere:theory and model simulation. J Biomech 37:1709–1718
99. Oster GF, Murray JD, Harris AK (1983) Mechanical aspects of mesenchymal morphogenesis. J Embryol Exp Morphol 78:83–125
100. Penelope CG, Janmey PA (2005) Cell type-specific response to growth on soft materials. J Appl Physiol 98:1547–1553
101. Isaksson H, Wilson W, van Donkelaar CC, Huiskes R, Ito K (2006) Comparison of biophysical stimuli for mechano-regulation of tissue differentiation during fracture healing. J Biomech 39(8):1507–16
102. Buxboim A, Ivanovska IL, Discher DE (2010) Matrix elasticity, cytoskeletal forces and physics of the nucleus: how deeply do cells 'feel' outside and in? J Cell Sci 123:297–308
103. Fu J, Wang YK, Yang MT, Desai RA, Yu X, Liu Z, Chen CS (2010) Mechanical regulation of cell function with geometrically modulated elastomeric substrates. Nature Methods 7:733–736
104. Zemel A, Rehfeldt F, Brown AE, Discher DE, Safran SA (2010) Optimal matrix rigidity for stress fiber polarization in stem cells. Nat Phys 6:468–473
105. Evans ND, Minelli C, Gentleman E, LaPointe V, Patankar SN, Kallivretaki M, Chen X, Roberts CJ, Stevens MM (2009) Substrate stiffness affects early differentiation events in embryonic stem cells. Eur Cell Mater 18:1–14
106. Burke DP, Kelly DJ (2012) Substrate stiffness and oxygen as regulators of stem cell differentiation during skeletal tissue regeneration: a mechanobiological model. PLoS ONE 7(7):e40737
107. Huang C, Dai J, Zhang XA (2015) Environmental physical cues determine the lineage specification of mesenchymal stem cells. Biochim Biophys Acta 1850(6):1261–6
108. Friedland JC, Lee MH, Boettiger D (2009) Mechanically activated integrin switch controls $\alpha 5\beta 1$ function. Science 323:642–44
109. Hera GJ, Wub HC, Chenc MH, Chene MY, Change SC, Wanga TW (2013) Control of three-dimensional substrate stiffness to manipulate mesenchymal stem cell fate toward neuronal or glial lineages. Acta Biomater 9(2):5170–80
110. Sabeh F, Shimizu-Hirota R, Weiss SJ (2009) Protease-dependent versus -independent cancer cell invasion programs: three-dimensional amoeboid movement revisited. J Cell Biol 185(1):11–9